Mathematical Biology

Check for updates

Dynamic modeling of bone remodeling, osteolytic metastasis and PK/PD therapy: introducing variable order derivatives as a simplification technique

Joana Pinheiro Neto[1,2] · Irina Alho[3] · Luís Costa[3] · Sandra Casimiro[3] ·
Duarte Valério[1] (iD) · Susana Vinga[1,4] (iD)

Abstract

Bone is constantly being renewed: in the adult skeleton, bone resorption and formation are in a tightly coupled balance, allowing for a constant bone density to be maintained. Yet this micro-environment provides the necessary conditions for the growth and proliferation of tumor cells, and thus bone is a common site for the development of metastases, mainly from primary breast and prostate cancer. Mathematical and computational models with differential equations can replicate this bone remodeling process. These models have been extended to include the effects of disruptive tumor pathologies in the bone dynamics, as metastases contribute to the decoupling between bone resorption and formation and to the self-perpetuating tumor growth cycle. Such models may also contemplate the counteraction effects of currently used therapies, and, in the case of treatments with drugs, their pharmocokinetics and pharmacodynamics. We present a thorough overview of biochemical models for bone remodeling, in the presence of a tumour together with anti-cancer and anti-resorptive therapy, formulated as systems of first-order differential equations, or simplified using variable order derivatives. The latter models, of which some are new to this paper, result in equations with fewer parameters, and allow accounting for anomalous diffusion processes. In this way, more compact and parsimonious models, that promptly highlight tumorous bone interactions, are achieved, providing an effective framework to counteract the loss of bone integrity on the affected areas.

✉ Duarte Valério
  duarte.valerio@tecnico.ulisboa.pt

Extended author information available on the last page of the article

🖄 Springer

1 Introduction

Bone tissue is constantly being renewed. Its remodeling is a dynamic, spatially heterogeneous process, for which several mathematical models have been proposed in the literature. Such models may concern only healthy bone tissue (Komarova et al. 2003; Lemaire et al. 2004; Komarova 2005; Pivonka et al. 2008; Ryser et al. 2009, 2010; Pivonka et al. 2010; Buenzli et al. 2011; Zumsande et al. 2011; Graham et al. 2013; Pivonka et al. 2013), or may include also the effects of tumors (Wang et al. 2011; Ryser et al. 2012); in the latter case, the effects of cancer treatments can be included too (Ayati et al. 2010; Araujo et al. 2014; Coelho et al. 2016a; Christ et al. 2016). This paper reviews those models and concentrates on those that employ fractional derivatives, i.e. models with derivatives of orders that are not necessarily integer (Christ et al. 2016). Such orders can, in fact, be fractional or irrational; they can also be time-varying. These variable order derivatives allow simpler formulations of the models (Neto et al. 2017a, b; Valério et al. 2019; Neto et al. 2019; Coelho et al. 2016b). This paper collects and reviews mostly published models, but the explicit consideration of variable order models for tumorous bone tissue, including the effects of available treatments for bone metastasis, including both anti-cancer and anti-resorptive therapies, as well as its spatial diffusion, and its pharmacokinetics (PK) and pharmacodynamics (PD) effects, is a novelty.

The remainder of this paper is organized as follows. Section 2 surveys the mechanisms of bone remodeling, explaining how it takes place. In Sect. 3, existing mathematical models, with integer order derivatives, for bone remodeling, metastasis and therapy are passed in review. Pharmacokinetics (PK) and pharmacodynamics (PD) control mechanisms of applied drugs are also included in this section. In Sect. 4, important mathematical formulations for fractional and variable order derivatives are introduced, focusing on Grünwald-Letnikoff constructions. In Sect. 5, variable order models are presented. The models which are novel in this paper are found here, in Sect. 5.2. Obtained simulation results are also discussed. Finally, conclusions and future work are summed up in Sect. 6.

2 Processes of bone remodeling

Bone remodeling takes place in cycles, which are regular, yet asynchronous. Such cycles affect at each instant 5 to 25 % of the total bone surface available (Crockett et al. 2011). Bone remodeling takes place in temporary anatomical structures within the bone, called Basic Multicellular Units (BMUs). In a BMU, bone is resorbed and then sequentially formed (Parfitt 1994). An active BMU can travel across the tissue at a constant speed of 20 to 40 μm/day, for up to 6 months. Autocrine and paracrine

factors controlled the interaction between the different clusters of bone cells tightly (Raggatt and Partridge 2010).

Bone degrading occurs due to multinucleated cells called *osteoclasts*. There are 10 to 20 osteoclasts in a BMU (Ryser 2011). These cells are the result of the fusion of mononucleated hematopoietic stem with progenitors cells, that express Receptor Activator of Nuclear Factor *k*B (*RANK*) and Macrophage Colony-stimulating Factor Receptor (*c-fms*). They differentiate into active osteoclasts, able to resorb bone, by biding to RANK-ligand (*RANKL*) and Colony-stimulating Factor 1 (*CSF-1*), respectively. Osteoclast performance is also due to osteoprotegerin (*OPG*), which is a soluble decoy receptor for RANKL, and a physiological negative regulator of osteoclastogenesis (Boyce 2012; Raggatt and Partridge 2010). BMU extension is due to the generation rate of osteoclasts. BMU life span determines the depth of the resorption (Bellido et al. 2014).

Bone formation occurs due to mononucleated cells called *osteoblasts*. There are 1000 to 2000 ostoblats in a BMU, secreting and depositing unmineralized bone matrix, directing its formation and mineralization into mature lamellar bone (Ryser 2011). Osteoblasts differentiate from mesenchymal stem cells (*MSC*). These are controlled, among other factors, by bone morphogenetic protein (*BMP*), Wnt-signaling, and vitamin D. Osteoblasts express parathyroid hormone (*PTH*) receptors. The expression of RANKL is upregulated by osteoblasts and cells of the osteoblastic lineage in response to PTH. RANKL binds to RANK, expressed in osteoclasts precursors, and promotes their activation (i.e. promotes bone resorption). Osteoclasts precursors also produce OPG, which binds to RANKL thus inhibiting osteoclastogenesis. OPG secretion is reduced in response to PTH, thereby furthering osteoclastogenesis. Osteoblasts can undergo apoptosis, differentiate into osteocytes, or differentiate into bone lining cells (Crockett et al. 2011; Roodman 2004).

PTH and the RANK/RANKL/OPG pathway are the principal regulators of bone resorption and formation. Bone remodeling can be activated by a mechanical stimulus on the bone, or due to systemic changes in homeostasis producing estrogen or PTH (Raggatt and Partridge 2010). The latter is triggered in response to a reduced calcium concentration. This leads to calcium release from the bone matrix. An elevated calcium concentration, on the other hand, inhibits the process (Silva and Bilezikian 2015). Bone remodeling begins when PTH triggers two mechanisms in the osteoblasts. First, existing PTH reduces osteoblasts secretion of OPG. OPG is a soluble decoy receptor for RANKL and thus allows it to bind to RANK. It promotes osteoclastogenesis in this way. Second, PTH receptors also upregulate the expression of RANKL. Again, RANKL binds to RANK, and this promotes osteoclast activation and bone resorption (Raggatt and Partridge 2010). How the formation phase is coupled to the resorption phase is not yet fully understood, since factors released from the bone matrix during resorption (Insulin Growth Factors I and II (*IGF-I*, *IGF-II*), and Transforming Growth Factor-β (*TGF-β*)) may be involved. Figure 1 shows a diagram of the healthy bone remodeling process. Bone formation takes place even in the presence of malfunctioning osteoclasts. This has led to the hypothesis that the coupling factors responsible for attracting and regulating osteoblasts to the sites of bone resorption are produced by osteoclasts (Boyce 2012). Osteoblasts begin forming bone at the resorbed site.
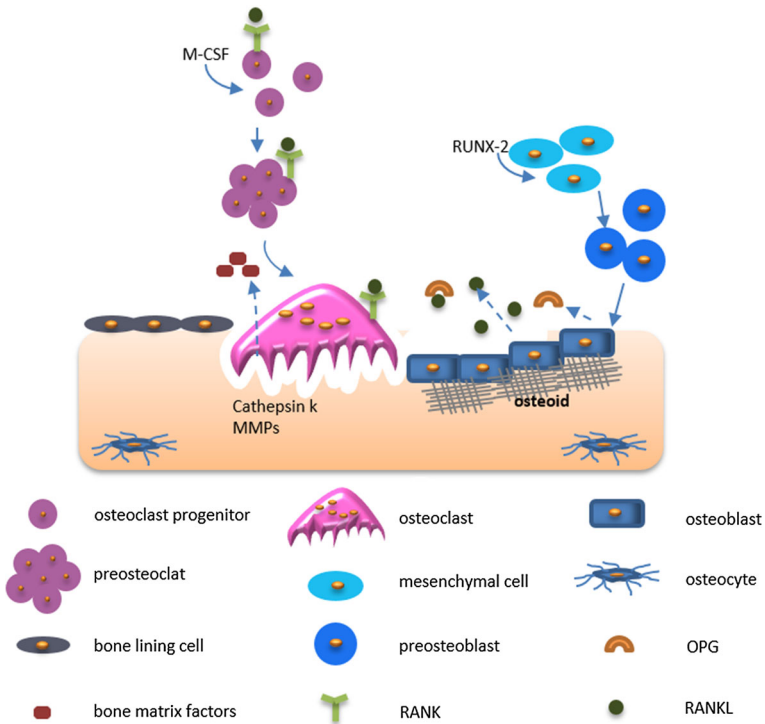
Fig. 1 Biochemical processes of healthy bone remodeling. For a healthy bone environment, PTH stimulates RANKL production by osteoblasts as the RANK/RANKL/OPG pathway plays an important role in bone resorption and formation. See also Fig. 2 for abnormal bone remodeling

Resorbed bone is replaced by the same amount of bone. This ends the bone remodeling cycle.

From this description it is seen that the BMU can be seen as a mediator mechanism. It bridges individual cellular activity to whole bone morphology (Raggatt and Partridge 2010).

Bone pathologies disrupt the biochemical regulation of bone remodeling. They can affect and deregulate it significantly. Consequently, bone integrity may be lost. Tumors have the capacity of spreading into organs other than its primary site. They often form metastasis in bone, according to the *seed* and *soil* hypothesis of Paget. Tumor cells interfere with the bone marrow to grow and proliferate. Sites of cancer metastasis are usually those where bone remodeling rates are high. The pelvis, the axial skeleton, or bones with abundant bone marrow are examples thereof (Boyce 2012; Schneider et al. 2005).

Bone metastases can be of two kinds. In osteolytic metastases, bone resorption is increased; in osteoblastic ones, bone formation is stimulated, but in an unstructured way. In both, bone resorption and formation take place but out of balance. Thus bone resistance and integrity decrease. Metastases in bone tissue originated from breast or prostate cancer often develop osteolytic or osteoblastic respectively (Suva et al. 2011).
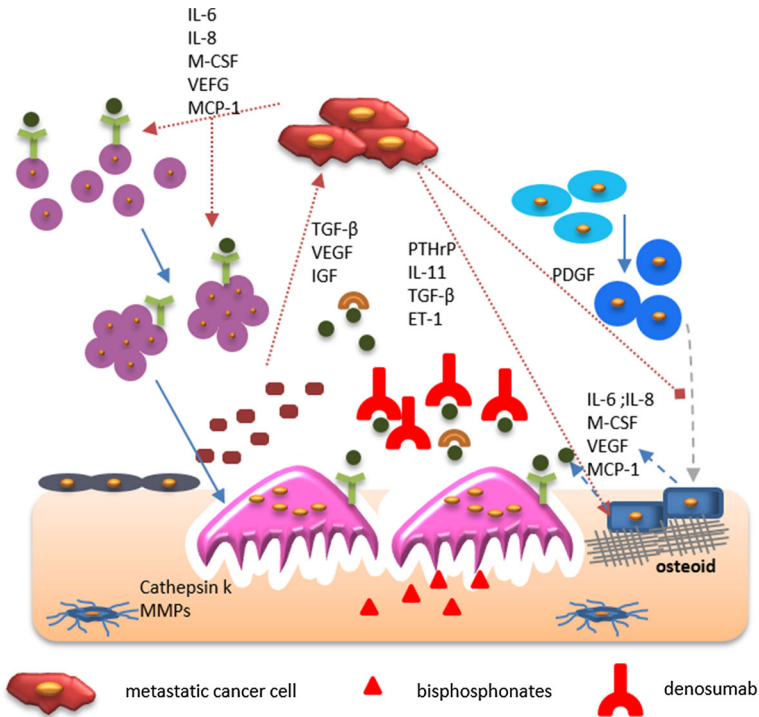
Fig. 2 Biochemical processes of abnormal bone remodeling. For the progression of osteolytic bone metastases, the vicious cycle is due to bone-derived tumor growth factors (IGFs,TGF-β, BMP, among others), tumor-derived factors that stimulate bone resorption (PTHrP, TGF-β, among others), and to tumor derived factors that affect bone formation (BMP, IGFs, among others) while PTHrP stimulates RANKL production by osteoblasts. See also Fig. 1 for healthy bone remodeling, and its caption for the symbols not explained in this figure

In the bone remodeling deregulation resulting from *osteolytic* metastases, tumor cells stimulate bone resorption (Chen et al. 2010; Huang et al. 2020). Considering the vicious cycle theory proposed in Mundy and Calcium (1998), cancer cells resident in bone can cause its destruction by stimulating osteoclast activity and receiving, in return, positive feedback from humoral factors released by the bone micro-environment during bone destruction (Casimiro et al. 2016). TGF-β is released from the bone matrix during resorption stimulating both tumor growth and parathyroid hormone-related protein (*PTHrP*) production in the cells of the metastasis. RANKL levels increase by binding to PTH receptors on cells of osteoblastic lineage. Osteoclasts are then activated, and this has two consequences: bone resorption increases (Casimiro et al. 2016), and TGF-β is released from the degraded bone. TGF-β further stimulates tumor growth and PTHrP secretion. Thus the vicious cycle is closed. This disruption of bone homeostasis is represented in Fig. 2.

In the bone remodeling deregulation resulting from *osteoblastic* metastases, tumorous cells grow because bone expresses endothelin-1 (*ET-1*), which stimulates osteoblasts by means of the endothelin A receptor (*ETR*), activating Wnt-signaling.

Tumor-derived proteases increase the release of osteoblastic factors, including TGF-β and IGF-I, from the extracellular matrix. Osteoblast activity induced by the tumor increases RANKL. This leads to PTH release and promotes osteoclast activity (Casimiro et al. 2016). Thus, the micro-environment of the tumor leads to the accumulation of new bone tissue.

There are different possible treatments of bone tumors, be they primary or methastatic. Treatments affect healthy cells as well. Thus a possible treatment strategy is to target not the tumor alone, but also the bone and its micro-environment (Li et al. 2019). In the case of an osteolytic metastatic bone disease, osteoclasts are targeted by anti-resorptive therapy, using *bisphosphonates* (such as alendronate or zoledronic acid) (Zometa 2017; Chen et al. 2002) and *monoclonal antibodies* (like denosumab) (Sohn et al. 2014; Gibiansky et al. 2012). Bisphosphonates lodge in bone and poison osteoclasts that degrade it. Monoclonal antibodies bind exclusively to RANKL, increase the OPG/RANKL ratio, and inhibit osteoclast formation. Therapies for other diseases such as multiple myeloma (*MM*) include daily doses of PTH, endothelin and proteasome inhibitors. These target osteoblasts to recover bone mass (Oyajobi et al. 2007). Anti-cancer agents (hormone therapy and chemotherapy such as paclitaxel Perez et al. 2001) that directly target metastatic and primary tumor cells are employed together with the aforementioned therapies (Casimiro et al. 2009).

The biochemical process of bone remodeling can be replicated through mathematical and computational models. The comparison of a healthy bone behavior with pathological states (Komarova et al. 2003; Ayati et al. 2010) was made possible, serving these models as clinical decision support systems for the implementation of therapeutic regimes (Ayati et al. 2010; Coelho et al. 2016a, 2015; Christ et al. 2016; Araujo et al. 2014). They consist of a system of ordinary differential equations that relate the interactions between osteoclasts and osteoblasts, by reproducing the effects of autocrine and paracrine control mechanisms. The resulting calculation of the dynamic response of these cells populations determines the changes in bone mass in the bone remodeling cycles. A local model, for healthy bone tissue, was initially proposed in Komarova et al. (2003) and further extended in Ayati et al. (2010) to include the influence of multiple myeloma (MM) disease and the counteraction of a treatment in the bone dynamics, based in proteasome inhibitors. It also proposed a non-local approach with diffusion.

Biological processes often present anomalous diffusion (Magin 2006), allowing for fractional derivatives to be introduced in the existing models (Sierociuk et al. 2013; Rahimy 2010). Many physical processes, however, also appear to exhibit a fractional order behavior that varies with time or space (Valério and Sá da Costa 2013; Lorenzo and Hartley 2002). Consequently, variable order derivatives can be introduced in the biochemical models of bone remodeling. This strategy, as a simplification technique, was already implemented in Neto et al. (2017a) and Neto et al. (2017b). Although models with more physiological details were proposed (reviewed below in Sects. 3.1 and 3.2), variable order derivatives were applied only to the simpler models of Komarova et al. (2003) and Ayati et al. (2010). However, the scope of applications of variable order derivatives is only expected to grow (Magin 2006).

All models presented here use dimensionless variables and parameters, including the cell populations, except when explicitly said otherwise in Table 2. D^1 refers to the

Table 1 Classification of the published models for *biochemical* bone remodeling, considering: H for a healthy bone environment; T for a tumor disrupted bone; and T&T for a bone tumor counteracted with therapy

Model by author	H	T	T&T
Komarova et al. (2003)	×	–	–
Komarova (2005)	×	–	–
Zumsande et al. (2011)	×	–	–
Graham et al. (2013)	×	–	–
Coelho et al. (2016a)	×	×	×
Ayati et al. (2010)*	×	×	×
Coelho et al. (2016a)	–	–	×
Christ et al. (2016)*	–	–	×
Lemaire et al. (2004)	×	–	–
Pivonka et al. (2010)	×	–	–
Pivonka et al. (2008)	×	–	–
Buenzli et al. (2011)*	×	–	–
Pivonka et al. (2013)*	×	–	–
Wang et al. (2011)	–	×	–
Ryser et al. (2009)*	×	–	–
Ryser et al. (2010)*	×	–	–
Ryser et al. (2012)*	–	×	–
Araujo et al. (2014)*	×	×	×

Term ***** indicates models with spatial evolution; indentation indicates development of a model in the previous level

first order derivative in time, $\frac{\mathrm{d}}{\mathrm{d}t}$ and $D^{\alpha(t)}$ or $D^{\alpha(t,x)}$ refers to the Grünwald-Letnikoff type-$\mathcal{D}$ variable order derivative, $\prescript{\mathcal{D}}{-\infty}{\mathrm{D}}_t^{\alpha(t)}$ or $\prescript{\mathcal{D}}{-\infty}{\mathrm{D}}_t^{\alpha(t,x)}$.

3 Models for bone remodeling using integer order derivatives

Mathematical and computational models can replicate the dynamics of bone remodeling, and its interaction with tumor cells. As a tool for an augmented experimental analysis, these models are important to simulate the biochemical processes occurring in the bone micro-environment that promote the progression of such disease (Pivonka and Komarova 2010).

Differential equations model the biochemical and biomechanical interactions in bone. Such models can be local or non-local; the latter are usually formulated in one-dimension, the extension to three-dimensions being trivial. Three cases can be consider: healthy bone, tumorous bone, and tumorous bone undergoing treatment. Table 1 provides a useful road-map into the published models.

In Sect. 3.1, several local models for bone remodeling dynamics found in the literature are reviewed. Section 3.2 does the same for non-local models. In Sect. 3.3, PK/PD relations are explained, as progress in understanding the genetic basis of cancer coupled to molecular pharmacology of potential new anticancer drugs calls for new approaches that are able to address key issues in the drug development process.

3.1 Local models

The very simple model of Komarova et al. (2003)

$$D^1 C(t) = \alpha_C C(t)^{g_{CC}} B(t)^{g_{BC}} - \beta_C C(t) \tag{1a}$$

$$D^1 B(t) = \alpha_B C(t)^{g_{CB}} B(t)^{g_{BB}} - \beta_B B(t) \tag{1b}$$

$$D^1 z(t) = -\kappa_C \max\left[0, C(t) - C_{ss}\right] + +\kappa_B \max\left[0, B(t) - B_{ss}\right] \tag{1c}$$

takes the form of an S-system (Savageau 1988). Exponents implicitly express biochemical autocrine (g_{CC}, g_{BB}) and paracrine (g_{BC}, g_{CB}) factors that couple the behavior of osteoclasts, $C(t)$, and osteoblasts, $B(t)$. The excess of $C(t)$ and $B(t)$ over their respective nontrivial steady states C_{SS} and B_{SS} determines the evolution of the bone mass density $z(t)$ through bone resorption and formation coefficients κ_C and κ_B. $\alpha_{C,B}$ and $\beta_{C,B}$ are the rates of production and death of the bone cells.

Depending on the values of autocrine and paracrine parameters, and in particular of the osteoblast-derived osteoclast paracrine regulator g_{BC} that implicitly represents the RANK/RANKL/OPG pathway, this model may represent a single remodeling cycle or periodic remodeling cycles, with amplitude and frequency determined by initial conditions. A deviation from the steady-state triggers the cycles. Simulation results for this model can be found in Fig. 3. Used parameters are the same as in Ayati et al. (2010) and presented in Table 3, as the osteoclast population triggered the periodical remodeling response by an increase 10 units above its steady-state.

In Komarova (2005), the anabolic and catabolic effects of the external administration of PTH are included, for a single remodeling cycle behavior of the model explained in Komarova et al. (2003). A bifurcation analysis to the generalized bone remodeling model is performed in Zumsande et al. (2011), and then applied to the models of Komarova et al. (2003), and extended incorporating osteoblasts precursors as a variable in the system. In Ryser et al. (2009), the influence of the OPG and RANKL concentrations were explicitly added into the system of Komarova et al. (2003). A parameter estimation and sensitivity analysis of this model is presented in Ryser et al. (2010). The original model of Komarova et al. (2003) was further extended in Graham et al. (2013). Osteocytes and pre-osteoblasts were included in the model, predicting an osteocyte induced bone remodeling, after the global apoptosis of a specific BMU. A new approach is presented in Lemaire et al. (2004), where the RANK/RANKL/OPG pathway, TGF-β and PTH were explicitly incorporated in the proposed model. Bone cells were mathematically encompassed as osteoblasts percursors, active osteoblasts and active osteoclasts, and their interaction is represented through the kinetic reaction of these molecules. Pivonka et al. (2008) extends the previous model to include bone mass dynamics and the production of both OPG and RANKL by the two types of osteoblastic lineage cells. Pivonka et al. (2010) provides a theoretical study on the role of the RANK/RANKL/OPG pathway in the system. It simulated several bone diseases by changing the values of the parameters, proposing treatment strategies for disturbances in this pathway.

More recently, Coelho et al. (2016a) proposed the integration of PTH into the model of Komarova et al. (2003), by adding a differential equation for its concentration. An
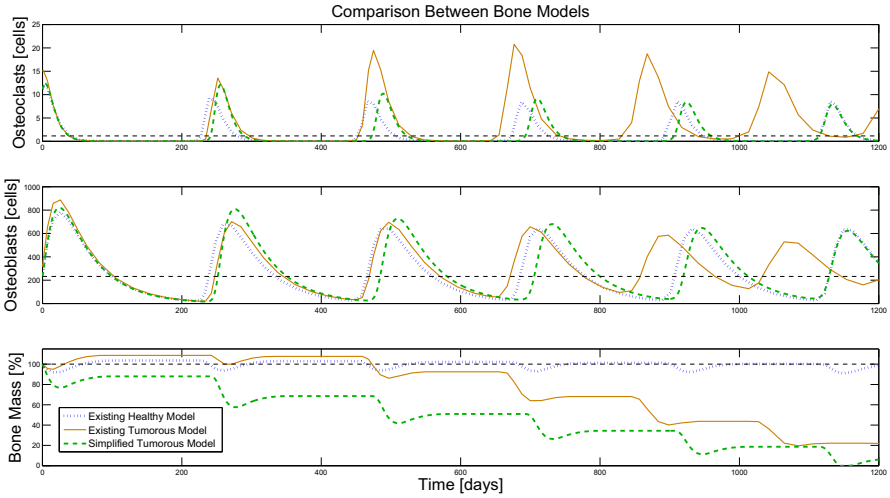
Fig. 3 Osteoclasts, Osteoblasts and Bone Mass evolutions, respectively. Dotted line: simulation of (1) for the existing model replicating a healthy bone micro-environment. Full line: simulation of (2), for a bone micro-environment disrupted by a developing tumor. Dashed line: simulation of the simplified tumorous model (16), considering the treatment parameters to be null, as in Neto et al. (2017b). Parameters were set according to Ayati et al. (2010), and can be found in Table 3. The variable order model was simulated with the same values as the healthy case, except the actualized resorption rate of $\kappa_C = 0.1548$, $\kappa_B = 6.4924 \times 10^{-4}$ for $R = 238.43$, and $\theta = 4 \times 10^{-8}$. Corresponding tumor evolution, equal for both model with metastases, can be found in the first graphic of Fig. 11

increase in PTH increases the production of RANKL by osteoblasts, thus affecting g_{BC} and initiating a single remodeling cycle.

The models can be adapted to include effects of pathologies. The model proposed in Ayati et al. (2010) extends the one in Komarova et al. (2003), incorporating in the bone dynamics the effect of MM:

$$D^1 C(t) = \alpha_C C(t)^{g_{CC}\left(1+r_{CC}\frac{T(t)}{L_T}\right)} B(t)^{g_{BC}\left(1+r_{BC}\frac{T(t)}{L_T}\right)} - \beta_C C(t) \tag{2a}$$

$$D^1 B(t) = \alpha_B C(t)^{\left(\frac{g_{CB}}{1+r_{CB}\frac{T(t)}{L_T}}\right)} B(t)^{\left(g_{BB}-r_{BB}\frac{T(t)}{L_T}\right)} - \beta_B B(t) \tag{2b}$$

$$D^1 T(t) = \gamma_T T(t) \log\left(\frac{L_T}{T(t)}\right) \tag{2c}$$

$T(t)$ is the density of tumor cells at time t, with a Gompertz form of constant growth $\gamma_T > 0$. The tumor affects the autocrine and paracrine regulation pathways through r_{ij} parameters. The effect of the tumor is assumed to be independent of the bone mass; periodic remodeling cycles are deregulated; bone mass density decreases. The maximum tumor size is L_T. The bone mass equation is the same of (1c) In Fig. 3, a simulation of the bone micro-environment for (2) can be found, for parameters set according to Ayati et al. (2010) and given in Table 3.

In Wang et al. (2011), the model of Pivonka et al. (2008) is also extended to include the influence of MM in the bone micro-environment. It was done by considering the disease vicious cycle results from the interaction between the bone micro-environment and MM cells, by explicitly including interleukin-6 (*IL-6*) and MM marrow stromal cell adhesion in the model. Coelho et al. (2016a) also allowed for the disruptive action of an osteolytic tumor to be included. Growth of bone metastasis, and its influence in the bone micro-environment, is achieved by encoding the production of PTHrP by the metastatic cells, when TGF-β is released from the bone in the resorption phase. Tumor treatment was also proposed. Proteasome inhibitors are known to have direct anti-myeloma effects and to have direct effect on osteoblasts, to stimulate osteoclast differentiation and bone formation. They were added into model proposed in Ayati et al. (2010), as two time dependent step functions.

In Coelho et al. (2015), a treatment of osteolytic bone metastases through anti-cancer and anti-resorptive therapy is proposed, adapting the model of Ayati et al. (2010) as presented in (3). It corresponds to the administration of two different chemotherapy ($d_{c_{34}}$) drugs combined with either bisphosphonates (d_2) or monoclonal antibodies (d_1). Bisphosphonates (e.g. zoledronic acid or alendronate) promote osteoclast apoptosis, and monoclonal antibodies (e.g. denosumab) indirectly inhibit osteoclast formation (Camacho and Jerez 2019) by acting as a decoy receptor for RANKL. Together with chemotherapy, the drug effect of this treatment was included in the model through their PK/PD action. The bone mass equation, $z(t)$, remains equal to (1c).

$$D^1 C(t) = \alpha_C C(t)^{g_{CC}\left(1+r_{CC}\frac{T(t)}{L_T}\right)} B(t)^{g_{BC}\left(1+r_{BC}\frac{T(t)}{L_T}\right)}(1+K_{s_1}d_1(t))$$
$$- \left(1 + K_{s_2}d_2(t)\right)\beta_C C(t) \tag{3a}$$

$$D^1 B(t) = \alpha_B C(t)^{\left(\frac{g_{CB}}{1+r_{CB}\frac{T(t)}{L_T}}\right)} B(t)^{\left(g_{BB}-r_{BB}\frac{T(t)}{L_T}\right)} - \beta_B B(t) \tag{3b}$$

$$D^1 T(t) = \left(1 - K_{i34}d_{c34}(t)\right)\gamma_T T(t) \log\left(\frac{L_T}{T(t)}\right) \tag{3c}$$

This treatment structure is also adpated in Coelho et al. (2016a), based on pharmacological PK/PD effect of anti-cancer and anti-resorptive therapy.

3.2 Non-local models

The previous models can be extended to include diffusion processes in the bone through partial differential equations.

Ayati et al. (2010) also extended its model to

$$D^1 C(t,x) = \sigma_C \frac{\partial^2}{\partial x^2}C(t,x) + \alpha_C C(t,x)^{g_{CC}} B(t,x)^{g_{BC}} -$$
$$- \beta_C C(t,x) \tag{4a}$$

$$D^1 B(t,x) = \sigma_B \frac{\partial^2}{\partial x^2}B(t,x) + \alpha_B C(t,x)^{g_{CB}} B(t,x)^{g_{BB}} -$$

$$- \beta_B B(t, x) \tag{4b}$$

$$D^1 z(t, x) = \sigma_z \frac{\partial^2}{\partial x^2} z(t, x) - \kappa_C \max[0, C(t, x) - \overline{C}_{SS}(x)] +$$
$$+ \kappa_B \max[0, B(t, x) - \overline{B}_{SS}(x)] \tag{4c}$$

allowing diffusion over one-dimension, $\sigma_i \frac{\partial^2}{\partial x^2}$, of osteoclasts, osteoblasts, and bone mass. These variables now depend on both t and $x \in [0, 1]$. The diffusion of z accounts for the stochastic nature of bone dynamics and not necessarily migration of cells.

MM influence was also added:

$$D^1 C(t, x) = \sigma_C \frac{\partial^2}{\partial x^2} C(t, x) - \beta_C C(t, x) +$$
$$+ \alpha_C C(t, x)^{g_{CC}\left(1 + r_{CC} \frac{T(t)}{L_T}\right)} B(t, x)^{g_{BC}\left(1 + r_{BC} \frac{T(t)}{L_T}\right)} \tag{5a}$$

$$D^1 B(t, x) = \sigma_B \frac{\partial^2}{\partial x^2} B(t, x) - \beta_B B(t, x) +$$
$$+ \alpha_B C(t, x)^{\left(\frac{g_{CB}}{1 + r_{CB} \frac{T(t)}{L_T}}\right)} B(t, x)^6 \left(g_{BB} - r_{BB} \frac{T(t)}{L_T}\right) \tag{5b}$$

$$D^1 T(t, x) = \sigma_T \frac{\partial^2}{\partial x^2} T(t, x) + \gamma_T T(t, x) \log\left(\frac{L_T}{T(t, x)}\right) \tag{5c}$$

Tumor cells undergo diffusion in $x \in [0, 1]$. The diffusion coefficient for the tumor is given by γ_T, which allows for its spatial growth. Regarding the bone mass equation, $z(t, x)$, the expression is the same as in (4c) and all variables are subjected to null Newmann boundary conditions. Initial conditions, now depending on x, can be found in Ayati et al. (2010). Simulations for a healthy and tumor bone micro-environment, for these non-local models, are presented in the first two rows of Fig. 4, respectively. The tumor evolution, with an initial development on the right side on the normalized bone, can be found in the second graphic of Fig. 11.

Christ et al. (2016) further extends the model of Ayati et al. (2010), adapted in Coelho et al. (2015), to include the PK/PD action of anti-cancer and anti-resorptive therapy, in a one-dimensional model:

$$D^1 C(t, x) = \sigma_C \frac{\partial^2}{\partial x^2} C(t, x) - \left(1 + K_{s_2} d_2(t)\right) \beta_C C(t, x) +$$
$$+ \alpha_C C(t, x)^{g_{CC}\left(1 + r_{CC} \frac{T(t)}{L_T}\right)} \times$$
$$\times B(t, x)^{g_{BC}\left(1 + r_{BC} \frac{T(t)}{L_T}\right)} \left(1 + K_{s_1} d_1(t)\right) \tag{6a}$$

$$D^1 B(t, x) = \sigma_B \frac{\partial^2}{\partial x^2} B(t, x) - \beta_B B(t, x) +$$
$$+ \alpha_B C(t, x)^{\left(\frac{g_{CB}}{1 + r_{CB} \frac{T(t)}{L_T}}\right)} \times$$

Healthy Bone Remodeling - [3]

Bone Remodeling with Tumor - [3]

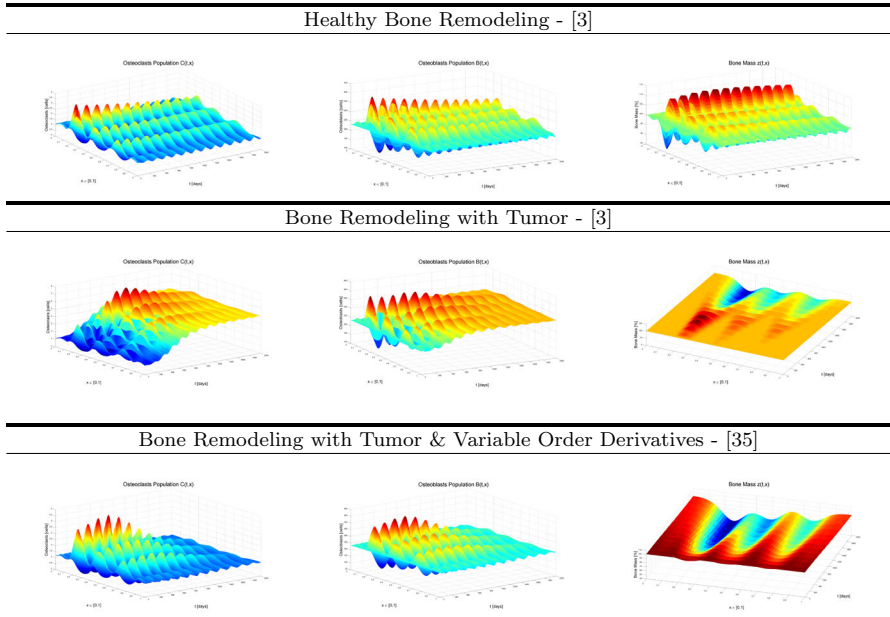Bone Remodeling with Tumor & Variable Order Derivatives - [35]

Fig. 4 Non-local simulation of Osteoclasts, Osteoblasts and Bone Mass. *Fisrt row*, for healthy remodeling cycles (4). *Second row*, for a tumor disrupted bone micro environment (5). *Third row*, for the simplified model for bone remodeling with tumor (15). Parameters, initial and boundary conditions follow exactly what was presented in Ayati et al. (2010), and can be found in Table 3. Variable order model parameters follow the integer healthy model values, except the actualized resorption rates of $\kappa_C = 0.1548$, $\kappa_B = 6.4924 \times 10^{-4}$ for $R = 238.43$ (equal for the analogous variable order local model), and $\theta = 2.5 \times 10^{-7}$. Untreated tumor evolution, for all metastases disrupted models, is presented in the second graphic of Fig. 11

$$\times B(t, x)^{\left(g_{BB} - r_{BB} \frac{T(t)}{L_T}\right)} \tag{6b}$$

$$D^1 T(t, x) = \sigma_T \frac{\partial^2}{\partial x^2} T(t, x) +$$
$$+ \left(1 - K_{i_{34}} d_{c_{34}}(t)\right) \gamma_T T(t, x) \log\left(\frac{L_T}{T(t, x)}\right) \tag{6c}$$

In Ryser et al. (2009), a spatial evolution of a single BMU was also included, and further extended in Ryser et al. (2012) to include the effect of bone metastasis in the remodeling process, as to study the ambiguous role of OPG in the system. From Pivonka et al. (2008), Buenzli et al. (2011) also added spatial evolution to different components of the model, introducing the appropriated fluxes in cells and regulatory agents. This model is able to capture the known organized structure of the BMU, presenting a resorption zone at the front, then a reversal zone, and how PTH and the RANK/RANKL/OPG pathway affects the bone cells in the different stages of maturation and during bone remodeling. Pivonka et al. (2013) proposed a model that takes into account biochemical, biomechanical and geometrical regulations, as it numerically investigates the influence of bone surface availability in bone remodeling. More

recently, Capacete ([2016]) proposed a combined approach. The interactions between bone cells are again described by ordinary differential equations, based on the work of Komarova et al. ([2003]) and Ayati et al. ([2010]), but also by a finite element model of a proximal femur to account for the mechanical stimulus in a bi-dimensional construction, based in Rubin et al. ([2006]). It was also extended to include the disruptive action of MM. On a different approach, Araujo et al. ([2014]) uses a Hybrid Cellular Automata to describe spatial and temporal interactions of bone cells and micro-environment, the viscious cycles imposed by prostate cancer metastases, and the effect of anti-resorptive treatment on the bone dynamics, though bisphosphonates and anti-RANKL therapy; Scheiner et al. ([2013]) includes the biomechanical regulation of bone remodeling and the treatment of osteoporosis by means ofthe PK/PD of monoclonal antibodies (denosumab).

3.3 Pharmacokinectics and pharmacodynamics (PK/PD)

Pharmacokinetic (PK) models are based on mass balance differential equations that characterize drug absorption and disposition within the body (Dhillon and Gill [2006]). For a one-compartment model for oral administration, the remaining drug concentration to be absorbed (C_g, in mg/L) and the effective drug concentration in the plasma (C_p, in mg/L) are described by

$$D^1 C_g = -\kappa_g C_g \tag{7a}$$

$$D^1 C_p = \kappa_g C_g - \kappa_p C_p \tag{7b}$$

where κ_g and κ_p are the absorption and elimination rates, respectively (Mager et al. [2003]).

For a single dosage drug of initial concentration C_0, the plasma concentration can be determined by ([8a]). For multiple doses, the plasma concentration of the nth dose is given by

$$C_p = C_0 \frac{\kappa_g}{\kappa_g - \kappa_p} (e^{-\kappa_p t} - e^{\kappa_g t}) \tag{8a}$$

$$C_p(n, t') = C_0 \frac{\kappa_g}{\kappa_g - \kappa_p} \left(\frac{1 - e^{-n\kappa_p \tau}}{1 - e^{-\kappa_p \tau}} e^{-\kappa_p t'} - \frac{1 - e^{-n\kappa_g \tau}}{1 - e^{-\kappa_g \tau}} e^{-\kappa_g t'} \right) \tag{8b}$$

Initial conditions are $C_0 = \frac{D_0 F}{V_d}$, administrated at equally spaced intervals $t' = t - (n-1)\tau$, where D_0 is the dosage, F the bioavailability, and V_d the volume distribution. Multiple dosage is governed by the steady-state $C_{pss} = \frac{C_0}{\tau \kappa_p}$. For a subcutaneous drug administration, the initial concentration is applied in the remaining drug to be absorbed ($C_g(0) = C_0$); for the intravenous case, the initial concentration goes directly to the concentration in the plasma ($C_p(0) = C_0$).

The Pharmacodynamic (PD) consists in a drug effect, $d(t) = \frac{C_p}{C_p^{50}(t)+C_p}$, that can be described by a Hill function depending on the drug's concentration (Pinheiro et al. 2011). It varies between 0 and 1, where $C_p 50(t) = f(t)C_p^{50/base}$ represents the concentration at 50% of its maximum effect, $C_p^{50/base}$ is the initial value of $C_p^{50}(t)$, and resistance to a drug can be described by $f(t) = 1 + K_r \int_0^t \max\left[0, L_r - C_p(\lambda)\right] d\lambda$ (Pinheiro et al. 2011).

Through the combination of pharmacokinetic and pharmacodynamic models, a PK/PD model for a drug is achieved. Since a drug pathway can have either an inhibitory (i: $-$) or a stimulatory (s: $+$) effect on a given metabolism, a control action (CA) to the tumorous presence in the mathematical models for bone remodeling is given by $CA(t) = 1 \pm K_{i,s}d(t)$. Constants $K_i, K_s > 0$ represent the maximum effect of a drug in a specific mechanism, with $d(t)$ being the PD response of a single drug or a combination of drugs.

4 Variable order derivatives

Fractional calculus generalizes differentiation and integration notions of order $n \in \mathbb{N}$ to that of orders $\alpha \in \mathbb{R}$. An appealing generalization is based on the exponential function, $D^n(e^{ax}) = a^n e^{ax}$, which suggests defining the derivative of order α, not necessarily integer, as $D^\alpha(e^{ax}) = a^\alpha e^{ax}$ (Valério and Sá da Costa 2013).

There are several alternative definitions for fractional derivatives (Ortigueira and Machado 2019). The definition considered here is the Grünwald-Letnikoff construction, based upon the usual definition of derivative $D^1 f(t) = \frac{df(t)}{dt} = \lim_{h \to 0} \frac{f(t)-f(t-h)}{h}$, from which it can be easily shown, using mathematical induction, that

$$D^n f(t) = \frac{d^n f(t)}{dt^n} = \lim_{h \to 0} \frac{\sum_{k=0}^n (-1)^k \binom{n}{k} f(t-kh)}{h^n}, \ n \in \mathbb{N} \qquad (9)$$

Since combinations $\binom{a}{b} = \frac{a!}{b!(a-b)!}$ can be redefined for arbitrary real numbers a and b as $\binom{a}{b} = \frac{\Gamma(a+1)}{\Gamma(b+1)\Gamma(a-b+1)}$ or $\binom{a}{b} = \frac{(-1)^b \Gamma(b-a)}{\Gamma(b+1)\Gamma(-a)}$, it is reasonable to define

$$_c D_t^\alpha f(t) = \lim_{h \to 0^+} \frac{\sum_{k=0}^{\lfloor \frac{t-c}{h} \rfloor} (-1)^k \binom{\alpha}{k} f(t-kh)}{h^\alpha}, \ \alpha \in \mathbb{R} \qquad (10)$$

where the upper limit of the summation ensures that the case $\alpha \in \mathbb{Z}^-$ is compatible with Riemann integrals, while the case $\alpha \in \mathbb{N}$ still gives the same result as (9).

This Grünwald-Letnikoff can be approximated as (11a), or, recursively, as (11b):

$$_0D_t^\alpha f(t) \approx \frac{1}{h^\alpha} \sum_{r=0}^{n} (-1)^r \binom{\alpha}{r} f(t-rh) \tag{11a}$$

$$_0^{rec}D_t^\alpha f(t) \approx \left(\frac{f(t)}{h^\alpha} - \sum_{r=1}^{n} (-1)^r \binom{-\alpha}{r} {}_0^r D_{t-rh}^\alpha f(t-rh) \right) \tag{11b}$$

In both cases, the step time is $h \in \mathbb{R}^+$, and $n = \lfloor t/h \rfloor$. If implemented for the entire length of the simulation, without any truncation of the series, both formulations are equivalent (Sierociuk et al. 2015c).

From all existing definitions, a common characteristic arises: operator D always depends on the integration limits c (here taken to be $c = 0$) and t. D is then a non-local operator and, consequently, it has memory of past values of $f(t)$ (Valério and Sá da Costa 2013).

Fractional calculus provides explicit expressions for new non-integer order dynamics. This characteristic makes it particularly well suited to describe the behavior of biological systems (e.g. subthreshold nerve conduction, viscoelasticity, bioelectrodes), since fractional derivatives occur most frequently, and naturally, in physical problems where the essential mechanisms, reactions, or interactions are governed by diffusion processes. Consequently, besides non-local spatial and prior temporal information, it also allows for anomalous diffusion to be mathematically described (Magin 2006).

The fractional order of integrals and derivatives can be a function of time or some other variable (Ortigueira et al. 2019; Lorenzo and Hartley 2002). Here, for time t, Grünwald-Letnikoff type-$\mathcal{D}$ formulation was used (Sierociuk et al. 2015a, b):

$$_0^{\mathcal{D}}D_t^{\alpha(t)} f(t) \approx \left(\frac{f(t)}{h^{\alpha(t)}} - \sum_{r=1}^{n} (-1)^r \binom{-\alpha(t)}{r} {}_0^{\mathcal{D}} D_{t-rh}^{\alpha(t)} f(t) \right) \tag{12a}$$

$$_{-\infty}^{\mathcal{D}}D_t^{\alpha(t)} f(t) \approx \left[\frac{f(t)}{h^{\alpha(t)}} - \right.$$
$$\left. - \sum_{j=1}^{n} (-1)^j \binom{-\alpha(t)}{j} \left({}_{-\infty}^{\mathcal{D}} D_{t-jh}^{\alpha(t-jh)} f(t) - c \right) + c \right] \tag{12b}$$

It can be approximated according to (12a). This derivative, successfully used for modeling the heat transfer process in a media with a time varying structure (Sierociuk et al. 2013), corresponds to an input-reductive strategy that assumes the rejection of input differentiators. That translates an immediate effect of order switching, schematically represented in Fig. 5. Additionally, this construction also allows for the effect of initial conditions having no memory of accumulated values, as formulated in (12b), where $_{-\infty}^{\mathcal{D}}D_l^\alpha f(t) = c = \text{const}$ for $l = (-\infty, 0)$. These characteristics are essential for the application of the type-$\mathcal{D}$ variable order definition to the bone remodeling models presented below.

Fig. 5 Schematic representation of the input-reductive switching order scheme, in serial form, from orders α_1 to α_2. From Sierociuk et al. (2015b)
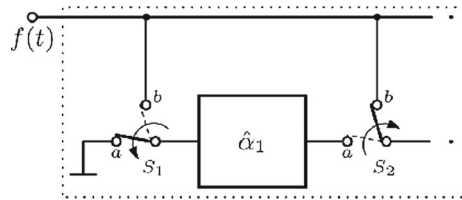
5 Simplified models for bone remodelling using variable order derivatives

Fractional and variable order derivatives have been already successfully used in modeling the dynamics of bone remodeling. Many dynamic relations in reality are fractional, even if that *fractionality* is very low (Petrás 2009). Consequently Christ et al. (2016) studied the effect of fractional derivatives in the model of Ayati et al. (2010). As to variable order derivatives, in Neto et al. (2017a, b) they have been introduced as a simplification technique in the same models of Ayati et al. (2010) and Coelho et al. (2015), in an effort to replicate the same bone micro-environment response but recurring to less parameters to imposed the known bone behavior. In fact, these tumor-disrupted bone remodeling models, as well as their extensions of Coelho et al. (2016a), Coelho et al. (2015) and Christ et al. (2016), can be simplified using variable order derivative methods.

In what follows, variable order models of bone remodelling are revisited in Sect. 5.1. The extension of these models to include the PK/PD action of combined anti-resorptive therapy is described in Sect. 5.2 (this extension is being published for the first time). Results and their discussion follow, in Sect. 5.3.

5.1 Revisiting simplified bone remodeling models

Fractional calculus allows considering orders not required to be integer numbers, which is specially adapted to describe biological processes with diffusion (Magin 2006). The same can be said for bone remodeling. However, introducing variable order derivatives also allows changing the dynamic response of a system, using less parameters to do so.

For the simplest biochemical model including the nefarious action of a tumor, type-$\mathcal{D}$ variable order derivatives were introduced in the cell populations of the bone micro-environment of Ayati et al. (2010). MATLAB/Simulink toolbox *Fractional Variable Order Derivative Simulink Toolkit* was used, where the buffer size is given by $n = \frac{t}{h}$, t being the simulation time, and h the sample time taken to be 1 day in all further addressed cases (Sierociuk et al. 2015b).

Considering that the tumor derived bone remodeling equations presented, either in their local version (2) or non-local version (5), are said to be independent of the bone micro-environment (Ayati et al. 2010), and that bone mass variations are but a reflection of osteoclasts and osteoblasts activity (Komarova et al. 2003), *a new model is formulated by changing the derivative's order of the osteoclasts and osteoblasts*

equations only, and by removing all r_{ij} coefficients. The variable order, $\alpha(t)$ or $\alpha(t, x)$, influenced by the tumor dynamics, is now responsible for inducing in the original healthy model, (1) and (4), the same response as the tumorous one, (2) and (5). This allows for a simpler model to represent the tumorous action in the bone dynamics, even when therapy is applied, (3) and (6).

The new equation associated with the required order format, for local and non-local scenarios, is

$$\alpha(t) = 1 - \theta \times t \times T(t) \tag{13a}$$

$$\alpha(t, x) = 1 - \theta \times t \times T(t, x) \tag{13b}$$

where θ is a constant term experimentally determined. Time t is related to the beginning of the tumor growth.

Since the resulting models' *steady-state, from a mathematical standpoint, is the same as the integer local healthy one's*, for all contemplated cases here, and most parameters remain with the same values used in Ayati et al. (2010), the associated activity of osteoclasts and osteoblasts in bone mass must differ from the original case. As such, the bone resorption-formation ratio, given by $R = \frac{\int_0^{\bar{t}} \max[0, C(t) - C_{SS}]}{\int_0^{\bar{t}} \max[0, B(t) - B_{SS}]}$, is determined; it assumes values between 0 and $\bar{t}$, and corresponds to the completion time of a single cycle of $C(t)$ in the new model (Ayati et al. 2010). Bone resorption and formation activities are then given by $\kappa_C = r R$ and $\kappa_B = r$, respectively. For the local case

$$D^{\alpha(t)} C(t) = \alpha_C C(t)^{g_{CC}} B(t)^{g_{BC}} - \beta_C C(t) \tag{14a}$$

$$D^{\alpha(t)} B(t) = \alpha_B C(t)^{g_{CB}} B(t)^{g_{BB}} - \beta_B B(t) \tag{14b}$$

$$D^1 z(t) = -\kappa_C \max\left[0, C(t) - C_{SS}\right] + \kappa_B \max\left[0, B(t) - B_{SS}\right] \tag{14c}$$

$$D^1 T(t) = \gamma_T T(t) \log\left(\frac{L_T}{T(t)}\right) \tag{14d}$$

$$\alpha(t) = 1 - \theta \times t \times T(t) \tag{14e}$$

simulation of the bone micro-environment (osteoclasts, osteoblasts and bone mass) can be found in Fig. 3. For comparison purposes, the results for the healthy and integer tumor disrupted bone remodeling versions of Ayati et al. (2010) are also presented. The tumor evolution remains the same, since it is considered independent of the bone micro-environment, even though such is not physiologically correct. The evolution can be found in the first graphic of Fig. 11.

Figure 6 allows a better analysis of the influence of θ in the order's expression. It is worth noticing that the numerical method used is extremely sensitive, as the order of the system is globally very close to 1. It is limited to values bigger than the magnitude of $\theta = 10^{-11}$, as is it not possible to run simulations with this value or smaller. For $\theta \geq 10^{-6}$ values the dynamic response is also not favorable, as it enhances the remodeling cycle period to values bigger than simulation time and with out-bounded amplitude. For $\theta = 10^{-7}$ the periodic dynamic response was recuperated.
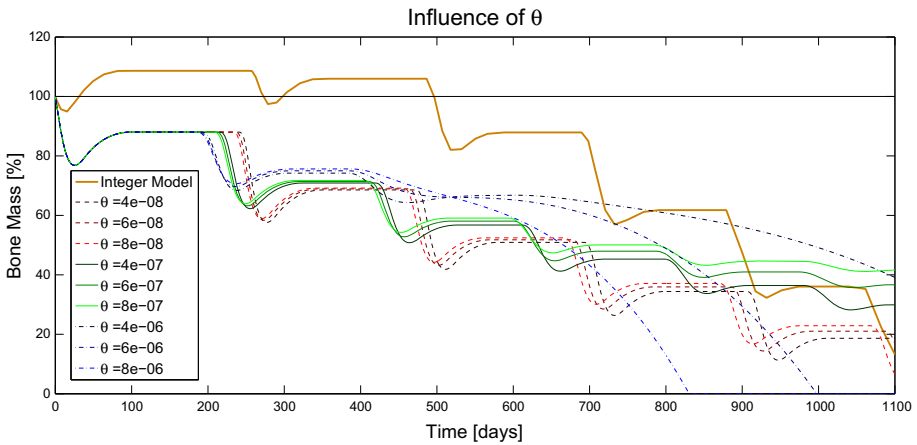
Fig. 6 Study of the influence of θ on the dynamic response of the simplified models (14)

The magnitude of $\theta = 10^{-8}$ was chosen but $\theta = 10^{-9}$ also reproduces qualitatively good results.

For the non-local case

$$D^{\alpha(t,x)}C(t,x) = \sigma_C \frac{\partial^2}{\partial x^2} C(t,x) - \beta_C C(t,x) +$$
$$+ \alpha_C C(t,x)^{g_{CC}} B(t,x)^{g_{BC}} \tag{15a}$$

$$D^{\alpha(t,x)}B(t,x) = \sigma_B \frac{\partial^2}{\partial x^2} B(t,x) - \beta_B B(t,x) +$$
$$+ \alpha_B C(t,x)^{g_{CB}} B(t,x)^{g_{BB}} \tag{15b}$$

$$D^1 z(t,x) = \sigma_z \frac{\partial^2}{\partial x^2} z(t,x) - \kappa_C \max[0, C(t,x) - C_{SS}] +$$
$$+ \kappa_B \max[0, B(t,x) - B_{SS}] \tag{15c}$$

$$D^1 T(t,x) = \sigma_T \frac{\partial^2}{\partial x^2} T(t,x) + \gamma_T T(t,x) \log\left(\frac{L_T}{T(t,x)}\right) \tag{15d}$$

$$\alpha(t,x) = 1 - \theta \times t \times T(t,x) \tag{15e}$$

simulation of the simplified model (15) can be found in the *third row* of Fig. 4, for the osteoclasts, osteoblasts and bone mass. Again for comparison purposes, in the *first row* healthy bone remodeling dynamics is presented, and in the *second row* integer tumor bone micro-environment with r_{ij} parameters. The tumor one-dimensional evolution can be found, again, in the first graphic of Fig. 11.

For either case, used parameters can be found in Table 3 (the same ones used in Ayati et al. (2010)), save for the values in the captions. Initial conditions with spatial distributions ($C(0, x)$ and $T(0, x)$) are the same used in Ayati et al. (2010), as are the boundary conditions.

In MM, osteoblast activity is known to be severely suppressed (Silbermann and Roodman 2012), which results in aggravated bone loss as osteoclasts are continuously promoted. However, in the results for the biochemical mathematical model presented not only in Ayati et al. (2010) as in the simplified models of this section, the bone forming cells still have some degree of action. Such behavior was considered in Neto et al. (2017a, b) to better fit a metastatic bone disease of osteolytic nature, such as a typical metastization to the bone of breast cancer (Holen (2012)), as achieved results for the bone micro-environment simulation were physiologically better described by such a new approach. It was also concluded in Neto et al. (2017a, b) that the variable order models provide qualitatively good results regarding both what is known of the bone micro-environment.

5.2 Therapy and variable order derivatives—a simplified extension

Both local and non-local version of the simplified model of Neto et al. (2017b) (14) and (15) can be extended to include therapy counteraction.

PK/PD of anti-cancer and anti-resorptive therapy was locally introduced in Coelho et al. (2015), to the models of Ayati et al. (2010), and further extended in Christ et al. (2016) to one dimensional geometries. Such models can be found in (3) and (6), that can be simplified by again removing all r_{ij} parameters and by adding a variable order to $C(t)$ and $B(t)$ (or to $C(t, x)$ and $B(t, x)$).

Given that the tumor base model of Ayati et al. (2010) is said to better describe an osteolytic metastatic bone disease, anti-cancer is combined with anti-resorptive therapy, instead of the initially proposed osteoblastic promotion based treatment for MM (Neto et al. 2017b; Coelho et al. 2015; Christ et al. 2016). Here, the effects of chemotherapy are given by $K_{i_3}d_3(t)$, considering the intravenous application of *paclitaxel* (Perez et al. 2001). It directly acts by targeting tumor cells, promoting their apoptosis in (3c) and (6c), and now in (16e) and (17d). Anti-resorptive therapy can be included using one of two possible treatments. Monoclonal antibodies, as *denosumab*, act as a decoy receptor for RANKL, lowering the RANKL concentration and hence the activation of osteoclasts. The term $K_{s_1}d_1(t)$ is consequently added to exponent g_{BC}, to represent the inhibition of RANKL produced by osteoblasts though the subcutaneous application of denosumab (Gibiansky et al. 2012; Sohn et al. 2014). Bisphosphonates, as zoledronic acid, lay on the bone matrix being released and absorbed by osteoclasts as they degrade bone. Bone resorption is then inhibited and osteoclast apoptosis promoted. Bisphosphonates are only considered to promote apoptosis of osteoclasts, influencing the β_C term.

The resulting simplified models are given by

$$D^{\alpha(t)}C(t) = \alpha_C C(t)^{g_{CC}} B(t)^{g_{BC}\left(1 + K_{s_1}d_1(t)\right)} -$$
$$- \left(1 + K_{s_2}d_2(t)\right)\beta_C C(t) \tag{16a}$$

$$D^{\alpha(t)}B(t) = \alpha_B C(t)^{g_{CB}} B(t)^{g_{BB}} - \beta_B B(t) \tag{16b}$$

$$D^{\alpha(t)}z(t) = -\kappa_C \max\left[0, C(t) - C_{SS}\right] +$$
$$+ \kappa_B \max\left[0, B(t) - B_{SS}\right] \tag{16c}$$

$$D^{\alpha(t)}T(t) = \left(1 + K_{i_3}d_3(t)\right)\gamma_T T(t) \log\left(\frac{L_T}{T(t)}\right) \tag{16d}$$

$$\alpha(t) = 1 - \theta \times t \times T(t) \tag{16e}$$

and

$$D^{\alpha(t,x)}C(t,x) = \sigma_C \frac{\partial^2}{\partial x^2}C(t,x) - \left(1 + K_{s_2}d_2(t)\right)\beta_C C(t,x) +$$
$$+ \alpha_C C(t,x)^{g_{CC}} B(t,x)^{g_{BC}\left(1 + K_{s_1}d_1(t)\right)} \tag{17a}$$

$$D^{\alpha(t,x)}B(t,x) = \sigma_B \frac{\partial^2}{\partial x^2}B(t,x) - \beta_B B(t,x) +$$
$$+ \alpha_B C(t,x)^{g_{CB}} B(t,x)^{g_{BB}} \tag{17b}$$

$$D^{\alpha(t,x)}z(t,x) = \sigma_z \frac{\partial^2}{\partial x^2}z(t,x) - \kappa_C \max\left[0, C(t,x) - C_{SS}(x)\right] +$$
$$+ \kappa_B \max\left[0, B(t,x) - B_{SS}(x)\right] \tag{17c}$$

$$D^{\alpha(t,x)}T(t,x) = \sigma_T \frac{\partial^2}{\partial x^2}T(t,x) +$$
$$+ \left(1 + K_{i_3}d_3(t)\right)\gamma_T T(t,x) \log\left(\frac{L_T}{T(t,x)}\right) \tag{17d}$$

$$\alpha(t,x) = 1 - \theta \times t \times T(t,x) \tag{17e}$$

When treatments are applied, however, the duration of an individual remodeling cycle is changed. Consequently, three resorption rates must be determined: when the tumor begins, R_{tumor}; when treatment is applied, R_{treat}; and when the tumor is extinguished and the treatment is consequently stopped, R_{healthy}. Each ratio is determined for the first complete cycle after the induced change. All involved variables and parameters are explained in Table 2. Non-local initial conditions, $C(0,x)$ and $T(0,x)$, are the same as presented in Ayati et al. (2010), as are the null Newmann boundary conditions applied to all variables in $x = 0$ and $x = 1$.

5.3 Results and discussion

For the local models of (16), simulation results can be found in Figs. 7 and 8, for chemotherapy combined with either denosumab (d_1) or zoledronic acid (d_2), respectively. Osteoclasts, osteoblasts, and bone mass are, for both cases, compared to the analogous integer order models. The tumor grows from $t = 0$ days, both treatments are applied at $t = 600$ days, and the tumor is considered extinct and the treatments are halted at $t = 2340$ days. Since the chemotherapy applied is always the same, the treated tumor evolution is presented in the first graphic of Fig. 11.

Non-local results from (17) are presented in the *second row* of both Figs. 9 and 10. Again, in the *first row*, analogous integer model results with r_{ij} parameters can be found for the osteoclasts, osteoblasts and bone mass. Figure 9 referrers to chemotherapy

Table 2 Summary and description of the variables and parameters for the proposed model (16) and (17)

	Description	Units
Variables		
t	Time	days
x	Distance	$x \in [0, 1]$
$C(t, x)$	Osteoclast population	–
$B(t, x)$	Osteoblast population	–
$z(t, x)$	Bone mass density	%
$T(t, x)$	Bone metastases density	%
$\alpha(t)/\alpha(t, x)$	Variable order expression	–
$d_1(t)$	Effect of denosumab	–
$d_2(t)$	Effect of zoledronic acid	–
$d_3(t)$	Effect of paclitaxel	–
Parameters		
α_C	OC activation rate	day^{-1}
α_B	OB activation rate	day^{-1}
β_C	OC apoptosis rate	day^{-1}
β_B	OB apoptosis rate	day^{-1}
g_{CC}	OC autocrine regulator	–
g_{BC}	OC paracrine regulator	–
g_{CB}	OB paracrine regulator	–
g_{BB}	OB autocrine regulator	–
κ_C	Bone resorption rate	day^{-1}
κ_B	Bone formation rate	day^{-1}
σ_C	Diffusion coefficient for OC	day^{-1}
σ_B	Diffusion coefficient for OB	day^{-1}
σ_z	Diffusion coefficient for bone mass	day^{-1}
σ_T	Diffusion coefficient for metastases	day^{-1}
r_{CC}	OC tumorous autocrine regulation	–
r_{BC}	OC tumorous paracrine regulation	–
r_{CB}	OB tumorous paracrine regulation	–
r_{BB}	OB tumorous autocrine regulation	–
L_T	Maximum size of bone metastases	%
γ_T	Metastases growth rate	% day^{-1}
$C(0)/C(0, x)$	Initial distribution of osteoclasts	–
$B(0)/B(0, x)$	Initial distribution of osteoblasts	–
$z(0)/z(0, x)$	Initial bone mass percentage	%
$T(0)/T(0, x)$	Initial tumorous mass percentage	%
C_{ss}	Steady-state OC number	–
B_{ss}	Steady-state OB number	–
D_0	Drug dosage	mg

Table 2 continued

	Description	Units
τ	Drug administration time interval	days
F	Bioavailability	–
V_d	Volume distribution	L
κ_g	Drug absorption rate	$days^{-1}$
κ_p	Drug elimination rate	$days^{-1}$
$C_p^{50/base}$	Initial drug concentration for 50% of its maximum effect	mg/L
K_r	Drug resistance capacity	–
K_{s1}	Maximum effect of denosumab	–
K_{s2}	Maximum effect of zoledronic acid	–
K_{i3}	Maximum effect of paclitaxel	–
θ	Variable order coefficient	–

Table 3 Variables and parameters, from Ayati et al. (2010), used for the simulations and equations of local and non local models presented in this paper, except when explicitly said otherwise

Unaltered Parameters			
α_C	3	σ_C	10^{-6}
α_B	4	σ_B	10^{-6}
β_C	0.2	σ_z	10^{-6}
β_B	0.02	σ_T	10^{-6}
g_{CC}	1.1	r_{CC}	0.005
g_{BC}	−0.5	r_{BC}	0
g_{CB}	1.0	r_{CB}	0
g_{BB}	0	r_{BB}	0.2
$z(0)/z(0,x)$	100	L_T	100
Local vs. non-local		Local	Non-local
κ_C		0.0748	0.45
κ_B		6.39×10^{-4}	0.0048
γ_T		0.005	0.004
$T(0)/T(0,x)$		1	*
Healthy vs. metastatic bone		Healthy	Metastatic
$C(0)/C(0,x)$		11.76*	15*
$B(0)/B(0,x)$		231.72	316
C_{ss}		1.16	5
B_{ss}		231.72	316

Constant parameters, regardless of the simulation type, are presented in the *Unaltered Parameters* section. Parameters that differ with local or non-local environments are presented in the *Local vs. Non-local* section. Healthy or metastatic bone parameters are presented in the *Healthy vs. Metastatic Bone* section

Table 4 Simulation parameters used for the local and non local models with PK/PD action of treatment, for (3) and (6): monoclonal antibodies, d_1 (denosumab), bisphosphonates, d_2 (zoledronic acid) and anti-cancer therapy, d_3 (paclitaxel)

Variables	d_1	d_2	d_1	Units
D_0	120	4	176	mg
τ	28	28	7	days
F	0.62	1	1	–
V_d	3.1508	536.3940	160.2570	L
κ_g	0.2568	–	–	days^{-1}
κ_p	0.0248	0.1139	1.2797	days^{-1}
$C_p^{50/base}$	1	0.0001	0.0002	mg/L
K_r	–	–	–	–
$K_{s,i}$	0.004	0.058	1.70	–

PK parameters (D_0, τ, F, V_d, κ_g, and κ_p), for denosumab can in found in Gibiansky et al. (2012), Sohn et al. (2014), zoledronic acid in Zometa (2017), Chen et al. (2002) and paclitaxel in Perez et al. (2001). PD parameters, $C_p^{50/base}$ and $K_{s,i}$, were chosen through simulation
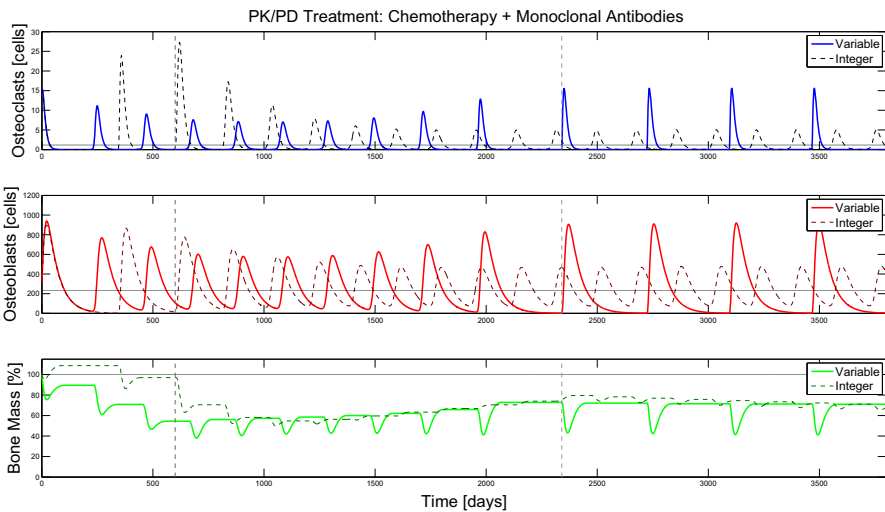

Fig. 7 Osteoclasts, Osteoblasts and Bone Mass evolutions, respectively, where treatment was applied combining chemotherapy (paclitaxel—d_3) with monoclonal antibodies (denosumab—d_1). The integer model, as presented in (3) (Coelho et al. 2015) and here adapted for the anti-resorptive therapy of Coelho et al. (2016a), is simulated in a *darker dashed line* (parameters in Table 3, for the metastatic case). For the new model proposed, the simulation of (16) is presented in a *light full line* (parameters in Table 3, for the healthy case; the order parameter was $\theta_{deno} = 8.25 \times 10^{-8}$, and the resorption rates were $R_{tumor} = 239.1189$, $R_{treat} = 101.44$, and $R_{healthy} = 123.26$, for $\kappa_C = 0.1548$). The corresponding tumor evolution, equal for both models with metastases, can be found in the *dashed line* in the first graphic of Fig. 11 (applied PK/PD chemotherapy is independent of the anti-resorptive therapy chosen), and used PK/PD parameters are presented in Table 4
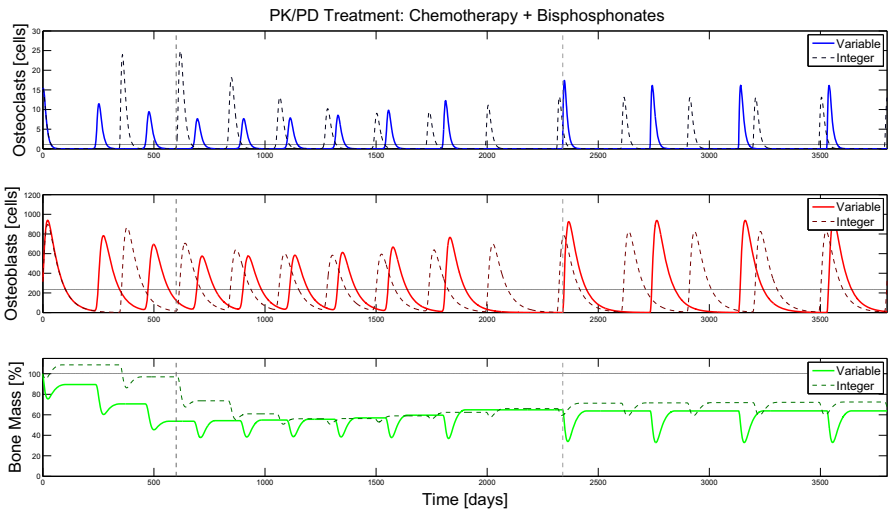
Fig. 8 Osteoclasts, Osteoblasts and Bone Mass evolutions, respectively, where treatment was applied combining chemotherapy (paclitaxel—d_3) with bisphosphonates (zoledronic acid—d_2). The integer model, as presented in (3) (Coelho et al. 2015) and here adapted for the anti-resorptive therapy of Coelho et al. (2016a), is simulated in a *darker dashed line* (parameters in Table 3, for the metastatic case). For the new model here proposed, the simulation of (16) is presented in a *light full line* (parameters in Table 3, for the healthy case; the order parameter was $\theta_{BP} = 6.034 \times 10^{-8}$, and the resorption rates were $R_{\text{tumor}} = 239.1189$, $R_{\text{treat}} = 97.98$, and $R_{\text{healthy}} = 123.26$, for $\kappa_C = 0.1548$). The corresponding tumor evolution, equal for both models with metastases, can be found in the *dashed line* in the first graphic of Fig. 11 (applied PK/PD chemotherapy is independent of the anti-resorptive therapy chosen), and used PK/PD parameters are presented in Table 4

(paclitaxel, d_3) combined with monoclonal antibodies (denosumab, d_1), and Fig. 10 to chemotherapy with bisphosphonates (zoledronic acid, d_2).

Regardless of the simulation, the resorption ratios R reflect what is known for each stage. As the tumor develops, the tightly coupled mechanism between resorption and formation is disrupted, as bone destruction is promoted by osteolytic metastases. Hence, R_{tumor} has a bigger value than in the remaining stages. When treatment is applied, it acts by generally inhibiting the osteoclastic action, which results in a lower value of R as formation is, consequently, promoted. When the tumor is extinct and treatment stopped, the resulting ratio is higher than the latter, as now healthy coupling is resumed regardless of the new stabilized value of z.

The value of θ slightly differs with the specified treatment, as d_1 (denosumab) acts through the S-system exponent g_{BC}, and d_2 (zoledronic acid) acts through the coefficent β_C. Translating from local to non-local, the order coefficient needs not to be adapted since the used θ is local simulations provides good results, not disturbed by acting diffusion processes. However, for all local and non-local cases, the order's magnitude is higher then the untreated tumor bone model counterpart.

For the local models, and overall consequence of introducing variable order derivatives results in wider remodeling cycles, and that the tumor acts more severely in beginning of the simulation but with a slower development. With both denosumab and zoledronic acid, osteoclasts see their number slightly diminish with an opposed
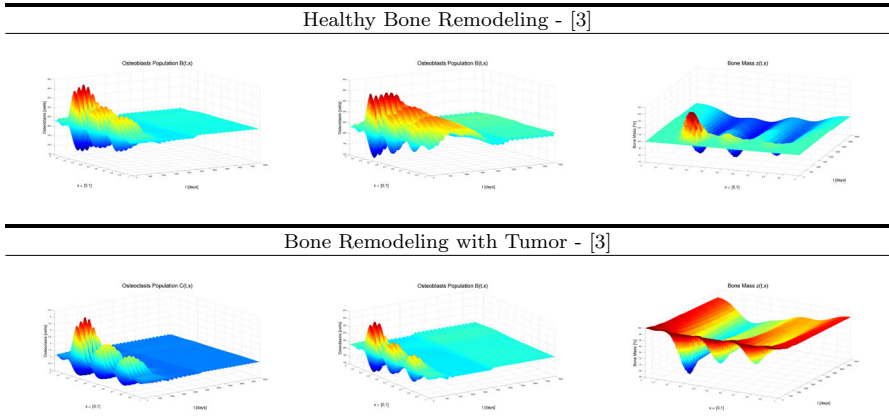
Healthy Bone Remodeling - [3]

Bone Remodeling with Tumor - [3]

Fig. 9 Non-local simulation of Osteoclasts, Osteoblasts and Bone Mass, for an applied PK/PD treatment of anti-cancer (chemotherapy—paclitaxel d_3) and anti-resorptive therapy (monoclonal antibodies—denosumab d_1) with parameters given in Table 4. *First* row, integer model simulation of (6), as presented in Christ et al. (2016) with $d_{c_{34}} = d_3$. *Second* row, proposed simplified variable order model of (17). Parameters, initial and boundary conditions follow exactly what was presented in Ayati et al. (2010), and can be found in Table 3. Variable order model parameters follow the integer healthy non-local model values, except the actualized resorption rates of $R_{\text{tumor}} = 239.1189$, $R_{\text{treat}} = 93.21$, and $R_{\text{healthy}} = 98.56$, for $\kappa_C = 0.1548$, and $\theta_{deno} = 4 \times 10^{-7}$. The corresponding tumor evolution, for either the integer or the variable order models, is presented in the third graphic of Fig. 11
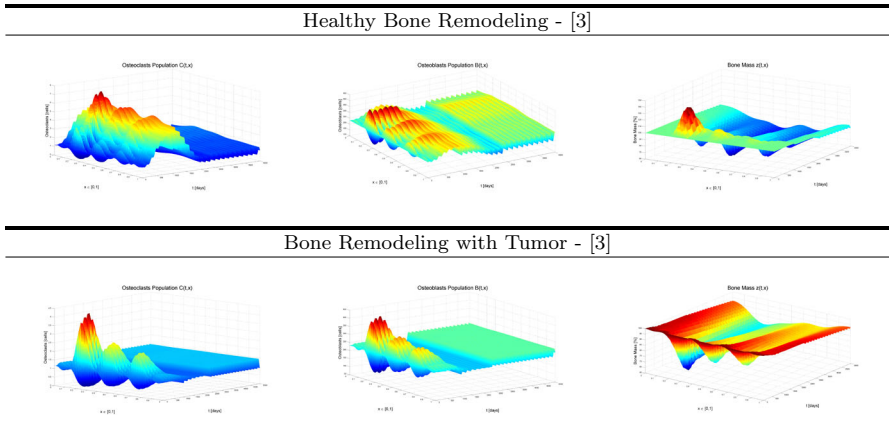
Healthy Bone Remodeling - [3]

Bone Remodeling with Tumor - [3]

Fig. 10 Non-local simulation of Osteoclasts, Osteoblasts and Bone Mass, for an applied PK/PD treatment of anti-cancer (chemotherapy—paclitaxel d_3) and anti-resorptive therapy (bisphophonates—zoledronic acid d_2) with parameters given in Table 4. *First* row, integer model simulation of (6), as presented in Christ et al. (2016) with $d_{c_{34}} = d_3$. *Second* row, proposed simplified variable order model of (17). Parameters, initial and boundary conditions follow exactly what was presented in Ayati et al. (2010), and can be found in Table 3. Variable order model parameters follow the integer healthy non-local model values, except the actualized resorption rates of $R_{\text{tumor}} = 239.1189$, $R_{\text{treat}} = 93.21$, and $R_{\text{healthy}} = 98.56$, for $\kappa_C = 0.1548$, and $\theta_{BP} = 6 \times 10^{-7}$. The corresponding tumor evolution, for either the integer or the variable order models, is presented in the third graphic of Fig. 11
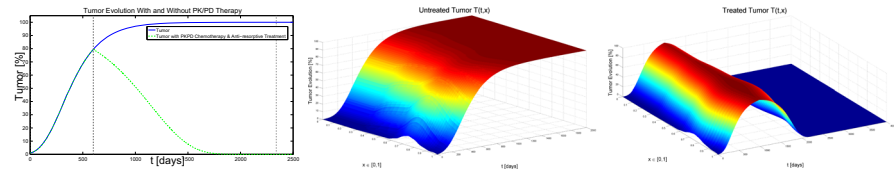
Fig. 11 Local and non-local tumor evolution. *First* graphic, local tumor evolutions are presented for chemotherapy treatments, (2c) and (14d), and for the untreated case, (16d). *Second* graphic, untreated spatial tumor evolution for an initial location on the right side of the normalized bone, (5c) and (15d) . *Third* graphic, tumor counteracted with the PK/PD chemotherapy action of paclitaxel (17d). Anti-tumor therapy parameters, either local or non-local, follow Table 4

reaction from the osteoblasts. As a consequence, bone mass stabilizes with very small recuperation, which reflects the nefarious action of an ostelytic tumor in the bone micro-environment. For the non-local cases, the same behavior is replicated.

As a conclusion, these simplified models mimicking bone behavior, tumorous action, and therapy counteraction, extending Neto et al. (2017a, b) to include therapy counter-action for an osteolytic metastization to the bone, can be said—even though they do not replicate the analogous integer case results precisely—to be qualitatively accurate. They are in accord with the known characteristics of the bone micro-environment response, namely the oscillations around homeostatic equilibrium and their amplitude and period (Komarova et al. 2003; Ayati et al. 2010). They are also in accord with the known characteristics of the bone micro-environment dynamics disrupted by an osteolytic tumor, namely the way how homeostatic equilibrium is affected by the tumor, and slowly recuperated by treatments (Casimiro et al. 2016; Ryser et al. 2012). The selected therapy employed is based on a combination of anti-cancer (chemotherapy—paclitaxel) with anti-resoprtive treatment (bisphosphonates—zoledronic acid; monoclonal antibodies—denosumab). The main goal of these models is to replicate analogous integer model results, with less parameters: an overall counting gives 1 equation added, for the system's order $\alpha(t)/\alpha(t, x)$, and 3 parameters suppressed, as all four r_{ij} were removed and θ was added to the order's equation. Hence, it can be concluded that variable order derivatives are a powerful tool that can be used to adequately replicate bone behavior.

6 Conclusions and future work

While detailed experimental data sufficient to quantitatively validate all the models passed in review in this paper does not yet exist, we have shown that the behavior obtained reproduces the characteristics of the physiological and clinical evolution of both disease and treatment. For this reason, biochemical models for bone remodeling, which are based upon existing knowledge of biochemical processes involved, are also expected to provide further valuable insights about the bone complex system. These models are also necessary to support the development of clinical decision systems for bone pathologies with efficient targeted therapies; in fact, control system techniques

can be used to tailor treatments for patients, if models accurate and reliable enough are available (Camacho and Jerez 2019).

This is why the computational analysis of bone physiological models is expected to have an impact on the development of clinical decision support systems in the future. Here are highlighted the road-map steps in an effort to bring that desired reality closer.

- Add diffusion terms, and consequent boundary conditions, for the PK/PD treatments prescribed, considering that, when a treatment is applied, it is done in a specific site and not uniformly in a region, regardless of intravenous or subcutaneous application methods;
- Add a more detailed tumor evolution, as it is here considered that tumor growth is independent of the bone micro-environment, which is physiologically incorrect;
- Applying the techniques here developed to models that include a more detailed and accurate description of the biochemical processes involved (Coelho et al. 2016a);
- Extending the models originally proposed in Komarova et al. (2003) and Ayati et al. (2010) to incorporate the biomechanical effects in the bone, which translates in adding mechanical solicitations in the original equations (Belinha et al. 2015; Capacete 2016), inasmuch such work would be simplified by using variable order derivatives in the resulting equations;
- Adapting these models to stochastic formulations such as those in Jerez and Cantó (2019);
- Finally, coefficients should be measured from experimental data, possibly data extrapolated from experiments with animals or *in vitro* experiments. The used parameters are not more than educated guesses by clinicians and oncobiologists at the magnitude of the values, leading to reasonable results from the qualitative point of view. Finding actual experimental values is probably the biggest challenge in the future.

References

Araujo A, Cook LM, Lynch CC, Basanta D (2014) An integrated computational model of the bone microenvironment in bone-metastatic prostate cancer. Cancer Res 74:813–817

Ayati BP, Edwards CM, Webb GF, Wikswo JP (2010) A mathematical model of bone remodeling dynamics for normal bone cell populations and myeloma bone disease. Biol Direct 5(1):28

Belinha J, Dinis LMJS, Natal Jorge RM (2015) The meshless methods in the bone tissue remodelling analysis. Proc Eng 110:51–58

Bellido T, Plotkin LI, Bruzzaniti A (2014) Chapter 2—bone cells. In: Basic and applied bone biology, chap. 2. Academic Press, pp 27–45

Boyce BF (2012) Bone biology ad pathology. In: Coleman R, Abrahamsson PA, Hadji P (eds) Handbook of cancer-related bone disease, 2nd edn. BioScientifica, pp 5–6

Buenzli PR, Pivonka P, Smith DW (2011) Spatio-temporal structure of cell distribution in cortical bone multicellular units: a mathematical model. Bone 48:918–926

Camacho A, Jerez S (2019) Bone metastasis treatment modeling via optimal control. J Math Biol 78(1–2):497–526

Capacete JDC (2016) Biochemical and biomechanic integrated modeling of bone. Master thesis, Instituto Superior Técnico

Casimiro S, Guise TA, Chirgwin J (2009) Molecular and cellular endocrinology the critical role of the bone microenvironment in cancer metastases. Mol Cellular Endocrinol 310:71–81

Casimiro S, Ferreira AR, Mansinho A, Alho I, Costa L (2016) Molecular mechanisms of bone metastasis: which targets came from the bench to the bedside? Int J Mol Sci 17:E1415

Chen T, Berenson J, Vescio R, Swift R, Gilchick A, Goodin S, LoRusso P, Ma P, Ravera C, Deckert F, Schran H, Seaman J, Skerjanec A (2002) Pharmacokinetics and pharmacodynamics of zoledronic acid in cancer patients with bone metastases. J Clin Pharmacol 42(11):1228–1236

Chen YC, Sosnoski DM, Mastro AM (2010) Breast cancer metastasis to the bone: mechanisms of bone loss. Breast Cancer Res BCR 12(6):215

Christ F, Valério D, Vinga S (2016) Modelling bone metastases using fractional derivatives (submitted)

Coelho RM, Vinga S, Valério D (2015) Cancersys—multiscale modeling for personalized therapy of bone metastasis. Tech. rep., Instituto Superior Técnico

Coelho RM, Lemos Ja M, Alho I, Costa L, Ferreira AR, Vinga S (2016a) Dynamic modeling of bone metastasis, microenvironment and therapy. integrating parathyroid hormone (PTH) effect, anti-resorptive and anti-cancer therapy. J Theor Biol 391:1–12

Coelho RM, Neto JP, Valério D, Vinga S (2016b) Dynamic biochemical and cellular models of bone physiology: integrating remodelling processes, tumor growth and therapy. In: Belinha J, Manzanares-Céspedes MC, Completo A (eds) The computational mechanics of bone tissue. Springer (2020) (in press)

Crockett JC, Rogers MJ, Coxon FP, Hocking LJ, Helfrich MH (2011) Bone remodelling at a glance. J Cell Science 124:991–998

Dhillon S, Gill K (2006) Basic pharmacokinetics. In: Clinical pharmacokinetics, 1st edn, chap 1. Pharmaceutical Press

Gibiansky L, Sutjandra L, Doshi S, Zheng J, Sohn W, Peterson M, Jang G, Chow A, Pérez-Ruixo J (2012) Population pharmacokinetic analysis of denosumab in patients with bone metastases from solid tumors. Clin Pharm 51(4):247–260

Graham JM, Ayati BP, Holstein SA, Martin JA (2013) The role of osteocytes in targeted bone remodeling: a mathematical model. PLoS ONE 8(5):E63884

Holen I (2012) Pathophysiology of bone metastases. In: Coleman R, Abrahamsson PA, Hadji P (eds) Handbook of cancer-related bone disease, 2nd edn. BioScientifica, p 49

Huang F, Cao Y, Wu G, Chen J, Wang C, Lin W, Lan R, Wu B, Xie X, Hong J, Fu L (2020) BMP2 signalling activation enhances bone metastases of non-small cell lung cancer. J Cellular Mol Med 24(18):10768–10784

Jerez S, Cantó JA (2019) A stochastic model for the evolution of bone metastasis: persistence and recovery. J Comput Appl Math 347:12–23

Komarova SV (2005) Mathematical model of paracrine interactions between osteoclasts and osteoblasts predicts anabolic action of parathyroid hormone on bone. Endocrinology 146(8):3589–3595

Komarova SV, Smith RJ, Dixon SJ, Sims SM, Wahl LM (2003) Mathematical model predicts a critical role for osteoclast autocrine regulation in the control of bone remodeling. Bone 33(2):206–215

Lemaire V, Tobin FL, Greller LD, Cho CR, Suva LJ (2004) Modeling the interactions between osteoblast and osteoclast activities in bone remodeling. J Theor Biol 229:293–309

Li RF, Zhang W, Man QW, Zhao YF, Zhao Y (2019) Tunneling nanotubes mediate intercellular communication between endothelial progenitor cells and osteoclast precursors. J Mol Hystol 50(5):483–491

Lorenzo CF, Hartley TT (2002) Variable fractional order and distributed order operators. Tech. Rep. February, National Aeronautics and Space Administration (NASA)

Mager DE, Wyska E, Jusko WJ (2003) Minireview on diversity of mechanism based pharmacodynamics models. Drug Metab Dispos 31(5):510–519

Magin RL (2006) Fractional calculus in bioengineering. Begell House Publishers Inc

Mundy GR, Calcium B (1998) Cancer and bone. Endocr Rev 19(1):18–54

Neto JP, Coelho RM, Duarte C, Vinga S, Sierociuk D, Malesza W, Macias M, Dzielinski A (2017) Variable order differential models of bone remodelling. In: 20th IFAC world congress. IFAC—International Federation of Automatic Control, Toulouse

Neto JP, Valério D, Vinga S, Sierociuk D, Dzielinski A (2017) Simplifying biochemical tumorous bone remodeling models through variable order derivatives (submitted)

Neto J, Valério D, Vinga S (2019) Variable-order derivatives and bone remodeling in the presence of metastases. In: Baleanu D, Lopes AM (eds) Handbook of fractional calculus with applications, vol 7. Applications in engineering, life and social sciences, part A. De Gruyter, pp 69–94

Ortigueira MD, Machado JT (2019) Fractional derivatives: the perspective of system theory. Mathematics 7(150)

Ortigueira MD, Valério D, Machado JT (2019) Variable order fractional systems. Commun Nonlinear Sci Numer Simul 71:231–243

Oyajobi B, O Garrett IR, Gupta A, Flores A, Esparza J, Muñoz S, Zhao M, Mundy G (2007) Stimulation of new bone formation by the proteasome inhibitor, bortezomib: implications for myeloma bone disease. Br J Haematol 139:434–438

Parfitt AM (1994) Osteonal and hemi-osteonal remodeling: the spatial and temporal framework for signal traffic in adult human bone. J Cellular Biochem 55(3):273–86

Perez EA, Vogel CL, Irwin DH, Kirshner JJ, Patel R (2001) Multicenter phase ii trial of weekly paclitaxel in women with metastatic breast cancer. J Clin Oncol 19(22):4216–4223

Petrás I (2009) Stability of fractional-order systems with frational orders: a survey. Int J Theory Appl 12(3)

Pinheiro JV, Lemos JM, Vinga S (2011) Nonlinear mpc of hiv-1 infection with periodic inputs.pdf. In: 50th IEEE conference on decision and control and European control conference (CDC-ECC), pp 65–70

Pivonka P, Komarova SV (2010) Mathematical modeling in bone biology: from intracellular signaling to tissue mechanics. Bone 47(2):181–189

Pivonka P, Zimak J, Smith DW, Gardiner BS, Dunstan CR, Sims NA, Martin TJ, Mundy GR (2008) Model structure and control of bone remodeling: a theoretical study. Bone 43(2):249–263

Pivonka P, Zimak J, Smith D.W, Gardiner B.S, Dunstan C.R, Sims N.A, Martin TJ, Mundy GR (2010) Theoretical investigation of the role of the rank/rankl/opg sistem in bone remodeling.pdf. J Theor Biol 262(2):306–316

Pivonka P, Buenzli PR, Scheiner S, Hellmich C, Dunstan CR (2013) The influence of bone surface availability in bone remodelling-a mathematical model including coupled geometrical and biomechanical regulations of bone cells. Eng Struct 47:134–147

Raggatt LJ, Partridge NC (2010) Cellular and molecular mechanisms of bone remodeling. J Biol Chem 285(33):25103–25108

Rahimy M (2010) Applications of fractional differential equations. Appl Math Sci 4(50):2453–2461

Roodman GD (2004) Mechanisms of bone metastasis. New England J Med 360(16):1655–1664

Rubin J, Rubin C, Jacobs CR (2006) Molecular pathways mediating mechanical signaling in bone. Gene 367:1–16

Ryser MD (2011) Of bones and noises. Ph.D. thesis, McGill University

Ryser MD, Nigam N, Komarova SV (2009) Mathematical modeling of spatio-temporal dynamics of a single bone multicellular unit. J Bone Mineral Res 24(5):860–870

Ryser MD, Komarova SV, Nigam N (2010) The cellular dynamics of bone remodeling: a mathematical model. SIAM J Appl Math 70(6):1899–1921

Ryser MD, Qu Y, Komarova SV (2012) Osteoprotegerin in bone metastases: mathematical solution to the puzzle. PLoS Comput Biol 8(10):E1002703

Savageau MA (1988) Introduction to s-systems and the underlying power-law formalism. Math Comput Modell II(3):546–551

Scheiner S, Pivonka P, Hellmich C (2013) Coupling systems biology with multiscale mechanics, for computer simulations of bone remodeling. Comput Methods Appl Mech Eng 254:181–196

Sierociuk D, Dzieliński A, Sarwas G, Petras I, Podlubny I, Skovranek T (2013) Modelling heat transfer in heterogeneous media using fractional calculus. Philos Trans Roy Soc 1–10

Schneider A, Kalikin LM, Mattos AC, Keller ET, Allen MJ, Pienta KJ, McCauley LK (2005) Bone turnover mediates preferential localization of prostate cancer in the skeleton. Endocrinology 146(4):1727–36

Sierociuk D, Malesza W, Macias M (2015a) Derivation, interpretation, and analog modelling of fractional variable order derivative definition. Appl Math Modell 39(13):3876–3888

Sierociuk D, Malesza W, Macias M (2015b) Fractional variable order derivative simulink user guide

Sierociuk D, Malesza W, Macias M (2015c) On the recursive fractional variable-order derivative: Equivalent switching strategy, duality, and analog modeling. Circ Syst Sig Process 34(4):1077–1113

Silbermann R, Roodman GD (2012) Bone health in myeloma. In: Coleman R, Abrahamsson PA, Hadji P (eds) Handbook of cancer-related bone disease, 2nd edn, chap 9. BioScientifica, pp 159–163

Silva B, Bilezikian J (2015) Parathyroid hormone: anabolic and catabolic actions on the skeleton. Curr Opin Pharmacol 22:41–50

Sohn W, Simiens MA, Jaeger K, Hutton S, Jang G (2014) The pharmacokinetics and pharmacodyamics of denosumab in patients with advanced solid tumors and bone metastases: a systematic review. Br J Clin Pharmacol 78(3):477–487

Suva LJ, Washam C, Nicholas RW, Griffin RJ (2011) Bone metastasis: mechanisms and therapeutic opportunities. Nat Rev Endocrinol 7(4):208–218

Valério D, Neto J, Vinga S (2019) Variable order 3D models of bone remodelling. Bull Polish Acad Sci Tech Sci 67(3):501–508

Valério D, Sá da Costa J (2013) An introduction to fractional control. Inst Eng Technol

Wang Y, Pivonka P, Buenzli PR, Smith DW, Dunstan CR (2011) Computational modeling of interactions between multiple myeloma and the bone microenvironment. PLoS ONE 6(11):E27494

Zometa® (2017) Zoledronic acid for injection. Novartis Pharmaceuticals Corporation, East Hanover, NJ

Zumsande M, Stiefs D, Siegmund S, Gross T (2011) General analysis of mathematical models for bone remodeling. Bone 48(4):910–917

Publisher's Note   Springer Nature remains neutral with regard to jurisdictional claims in published maps and institutional affiliations.

Authors and Affiliations

Joana Pinheiro Neto[1,2] · Irina Alho[3] · Luís Costa[3] · Sandra Casimiro[3] · Duarte Valério[1] · Susana Vinga[1,4]

✉ Duarte Valério
   duarte.valerio@tecnico.ulisboa.pt

   Joana Pinheiro Neto
   joana.neto@tecnico.ulisboa.pt

   Irina Alho
   ialho@medicina.ulisboa.pt

   Luís Costa
   luiscosta.oncology@gmail.com

   Sandra Casimiro
   scasimiro@medicina.ulisboa.pt

   Susana Vinga
   susanavinga@tecnico.ulisboa.pt

[1] IDMEC, Instituto Superior Técnico, Universidade de Lisboa, Av. Rovisco Pais 1, 1049-001 Lisbon, Portugal

[2] Present Address: CapGemini, Av. Colégio Militar 37F, Torre Colombo Oriente 10th floor, 1500-180 Lisbon, Portugal

[3] Instituto de Medicina Molecular, Faculdade de Medicina, Universidade de Lisboa, Av. Prof. Egas Moniz, 1649-028 Lisbon, Portugal

[4] INESC-ID, Instituto Superior Técnico, Universidade de Lisboa, R. Alves Redol 9, Lisbon 1000-029, Portugal